On the optimal acceleration of time-resolved 3D imaging using GRAPPA

B. A. Jung[1], S. Bauer[1], and M. Markl[1]
[1]Dept. of Diagnostic Radiology, Medical Physics, University Hospital, Freiburg, Germany

Introduction: Time-resolved 3D imaging often suffers from long acquisition times while aiming for high temporal or spatial resolution. To speed up acquisition times parallel imaging techniques for volumetric [1] and time-resolved 2D data acquisition have been introduced [2-4]. However, no systematic investigation of parallel imaging using GRAPPA to reconstruct time-resolved 3D data has been presented to date. Hence, the aim of this work was to explore how to optimally undersample and reconstruct time-resolved 3D data.

Methods: Imaging was performed on a 3T Siemens Trio system using a 12 channel head coil. The two phase encoding directions were left-right and anterior-posterior to ensure a symmetric coil configuration and exclude dependencies on coil geometry. Time-resolved 3D data was acquired in a moving phantom with an isotropic matrix of 64*64*64 and a voxel size of 2.4*2.4*2.4 mm^3 as well as with an anisotropic matrix of 128*128*40 also with isotropic voxel size of 1.6*1.6*1.6 mm^3. The temporal resolution was 47 ms, the motion range of the phantom ~4cm with a frequency of ~1.2Hz. Further, an additional noise-only measurement (matrix 128*128*48) with zero flip angle was performed to allow for SNR analysis.
PEAK-GRAPPA [4] as an extension of kt-GRAPPA (characterized by a uniform kernel geometry composing a smallest cell within the acquisition pattern in combination with temporal averaging of coil weights) was used for image reconstruction. An extended 4D-kernel (*kx,ky,kz,t*) as illustrated in Fig.1 was used to directly calculate a single set of coil weights for the entire 4D data set. This acquisition scheme was theoretically suggested for kt-SENSE reconstruction of 4D-data described by Tsao et al [5]. Further, reconstruction using a 3D-kernel (*kx,ky,t*) was performed to determining coil weights from $N_{ACS(y)}$ reference lines for each of the $N_{ACS(z)}$ reference partitions separately (W_i, $i=1:N_{ACS(z)}$). These were subsequently averaged to a single set of coil weights ($W=\sum W_i/N_{ACS(z)}$) to reconstruct all partitions separately (see Fig.2). For the isotropic matrix data 8*8 (reduction factor R=5) or 10*10 (R=10) ACS lines were used in ky- and kz-direction. The anisotropic data was reconstructed using 24*7 ACS lines (R=5 and R=10) in ky- and kz-direction to account for the anisotropic signal distribution in the ky-kz-space. Reconstruction using an alternative kernel approach with a smaller kernel extension (*bt=3* or *bz=3*) for R=10 as shown in Fig.3 was performed.
Image reconstruction was performed in Matlab while removing k-space lines retrospectively from the fully acquired k-space data according to the sampling patterns in Fig.1-3. Reference lines were copied back into the data matrix after reconstruction to preserve the temporal dynamics. Regional (encompassing the moving phantom) root-mean-square error (RMSE) averaged over the slices within the phantom and averaged over all time frames was determined as well as SNR within a ROI in the phantom using the zero flip angle scan.

Results: Phantom images of a frame during peak velocity are shown in Fig.4 for full k-space data, 3D- and 4D kernel configurations for the anisotropic data matrix with R=5 demonstrating a slightly degraded image quality for the 4D-kernel, also exhibiting a higher noise level, compared to the 3D-kernel reconstruction. Table 1 summarizes the error for the different reconstruction modalities: for the isotropic matrix the 4D-kernel configuration demonstrated a decreased error compared to the 3D-kernel reconstruction (7.0 vs 8.8% for R=5) whereas for the anisotropic matrix an opposite behaviour can be observed (13.3 vs 9.9% for R=5). For the higher reduction factor R=10 the 3D-kernel yields superior results for both data matrices. The SNR analysis confirms the behaviour as can be seen in Fig.4: the 3D-kernel yields an SNR of 30.9 and the 4D-kernel of 19.3 with R=5 and 24*7 ACS lines (SNR reference =36.5). Slightly better results can be obtained for the isotropic data reducing the kernel extension (10.2% for *bt=3* and 8.3% for *bz=3*). However, no superior results are obtained with the anisotropic matrix.

Discussion: By including additional dimensions, especially the temporal domain, in the PEAK-GRAPPA reconstruction process, considerably improved image quality for time-resolved 3D imaging can be reached for high acceleration factors compared to conventional parallel imaging. However, the results indicate that the choice of the (multi-dimensional) GRAPPA kernel (characterized by various degrees of freedom) has a strong impact on the quality of the image reconstruction. The definition of an optimal undersampling pattern and reconstruction kernel is thus not a straightforward problem. For a symmetric data matrix, it has been demonstrated that the 4D-kernel configuration leads to better results in terms of the error behaviour. However, in a more realistic anisotropic data matrix typically used in clinical applications the different kernel configurations show an opposite behaviour. Further, using a 4D-kernel configuration yields a decreased SNR compared to the 3D-configuration. Further investigations should investigate the dependency of different coil configurations and spatial resolution on the reconstruction quality in more detail. The aim is to identify application specific kernel configurations f to optimize multi-dimensional data acquisition such 4D-cardiac breathhold imaging or 4D-flow imaging.

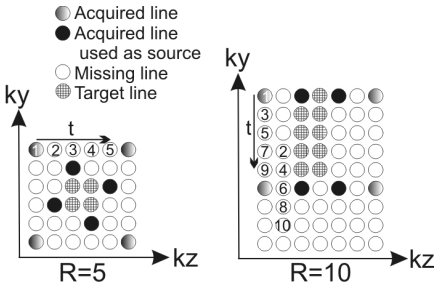

Fig.1: Optimized 3D-sampling pattern (ky,kz,t) according to Tsao et al [5] with its source and target points used for the PEAK-GRAPPA reconstruction. The pattern is shifted along the temporal domain according to the numbers. The kernel also incudes target points in the temporal domain (not shown). This leads e.g. for R=5 to 8 source and 4 target points.

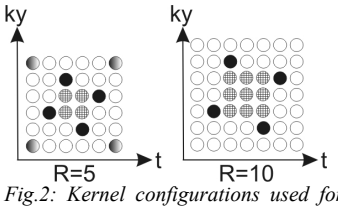

Fig.2: Kernel configurations used for the 3D-kernel reconstruction (see Methods section).The same pattern is acquired for all partitions.

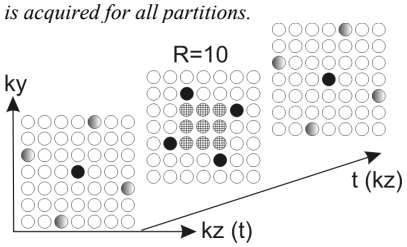

Fig.3: Alternative kernel approaches for R=10.

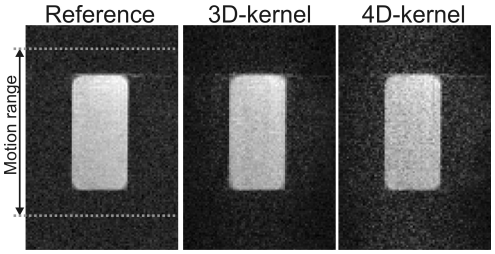

*Fig.4: Images of the moving phantom showing a frame during peak velocity for the different kernel configurations (matrix=128*40; R=5).*

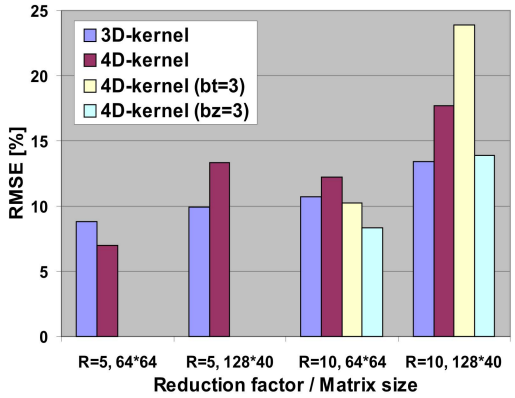

Fig.5:RMSE for the different kernel configu-rations, data sets, and R. 3D-kernel belongs to Fig.2, 4D-kernel to Fig.1 and 4D-kernel with bt=3 or bz=3 belongs to Fig.3

References: [1] Breuer et al. *MRM* 2006;55:549-55. [2] Tsao et al. *MRM* 2003;50:1031-42. [3] Huang et al. *MRM* 2005;54:1172-84. [4] Jung et al. *JMRI* 2008; 28:1226-32. [5] Tsao et al. *MRM* 2005; 53:1372–82.
Acknowledgements: Bundesministerium für Bildung und Forschung (BMBF), Grant # 01EV0706.